

# Multimode bolometer development for the Primordial Inflation Explorer (PIXIE) instrument

---



Peter C. Nagler <sup>1,2</sup>

Kevin T. Crowley <sup>3</sup> Kevin L. Denis <sup>1</sup> Archana M. Devasia <sup>1,4,5</sup> Dale J. Fixsen <sup>1,4</sup>

Alan J. Kogut <sup>1</sup> George Manos <sup>1</sup> Scott Porter <sup>1</sup> Thomas R. Stevenson <sup>1</sup>

June 30, 2016

<sup>1</sup>NASA/GSFC

<sup>2</sup>Brown University

<sup>3</sup>Princeton University

<sup>4</sup>University of Maryland

<sup>5</sup>CRESST

# Outline

1. Introduction and instrument description
2. Detector design and fabrication
3. Package and readout
4. Detector performance
5. Conclusions



# **Introduction and instrument description**

---

# Introduction

The Primordial Inflation Explorer (PIXIE) [1, 2]

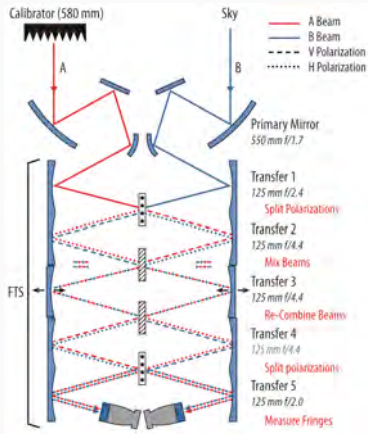
- Space-based polarizing Fourier transform spectrometer (FTS).
- Designed to measure the polarization and intensity spectra of the CMB.
- Multimode “lightbucket” design enables nK-scale sensitivity across 2.5 decades in frequency with just 4 thermistor-based bolometers.
- Like other FTSs [3, 4, 5, 6], PIXIE’s design and experimental approach<sup>a</sup> represent a significant departure from imagers often used for CMB measurements. *This is especially true for the detectors.*
  - Large etendue ( $A\Omega = 4 \text{ cm}^2 \text{ sr}$ ).
  - Handle large optical load (120 pW).
  - Large and mechanically robust absorber structure (30x larger than the spider web bolometers on Planck [7]).
  - Limited sensitivity to particle hits.
  - Sensitive to all optical frequencies of interest (15 GHz - 5 THz).
  - Photon-noise limited ( $\text{NEP} \leq 1 \times 10^{-16} \text{ W}/\sqrt{\text{Hz}}$ ).

---

<sup>a</sup>See Al Kogut’s poster on systematic error mitigation and Dale Fixsen’s talk on beams.



# Instrument description



Each focal plane has two polarization-sensitive bolometers mounted back-to-back with their polarization axes orthogonal.

Incident radiation:

$$\vec{E}_{inc} = A\hat{x} + B\hat{y} \quad (1)$$

Measured power:

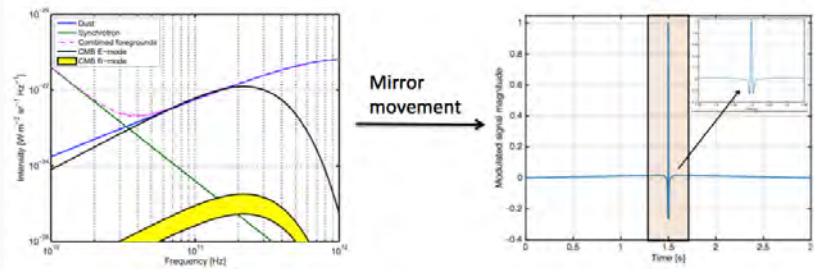
$$\begin{aligned} P_x^L &= \frac{1}{2} \int (A^2 + B^2) + (A^2 - B^2) \cos\left(\frac{4\nu z}{c}\right) d\nu. \\ P_y^L &= \frac{1}{2} \int (A^2 + B^2) + (B^2 - A^2) \cos\left(\frac{4\nu z}{c}\right) d\nu. \\ P_x^R &= \frac{1}{2} \int (A^2 + B^2) + (A^2 - B^2) \cos\left(\frac{4\nu z}{c}\right) d\nu. \\ P_y^R &= \frac{1}{2} \int (A^2 + B^2) + (B^2 - A^2) \cos\left(\frac{4\nu z}{c}\right) d\nu. \end{aligned} \quad (2)$$

Inverse Fourier transform:

$$\begin{aligned} S_x^L(\nu) &= A_\nu^2 - B_\nu^2. \\ S_y^L(\nu) &= B_\nu^2 - A_\nu^2. \\ S_x^R(\nu) &= A_\nu^2 - B_\nu^2. \\ S_y^R(\nu) &= B_\nu^2 - A_\nu^2. \end{aligned} \quad (3)$$

*Signal = small modulated component in a bright ( $\sim 120$  pW) background.*

# Instrument description



- Mirror position  $z \rightarrow$  optical path difference  $\ell$ :  $z \simeq \ell/4$ .
- Mirror velocity  $v$ :  $v = z / (3 \text{ sec}) = 1.73 \text{ mm/sec}$ .
- Optical path difference  $\ell \rightarrow$  interfering radio frequency  $\nu$ :  $\ell = c/\nu$ .
- Radio frequency  $\nu \rightarrow$  Audio (FTS) frequency  $\omega$ :  $\omega = 4\nu v/c$ .
- CMB:  $\omega \lesssim 15 \text{ Hz}$ .
- Dust:  $\omega \lesssim 100 \text{ Hz}$ .

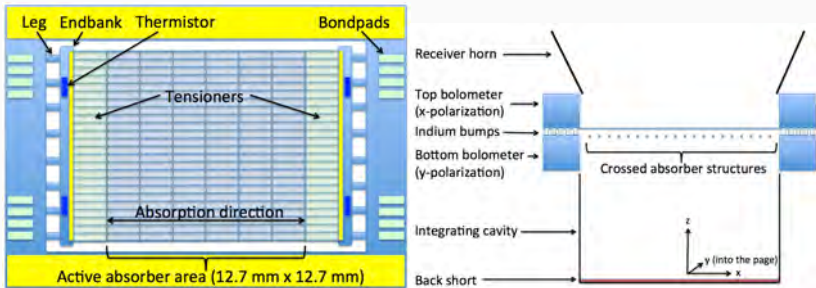
These constraints drive the bolometer bias and bandwidth requirements.

*Detectors must be photon noise limited across all FTS frequencies (0 – 100 Hz) under large, near-constant ( $\sim 120 \text{ pW}$ ) optical bias.*

# Detector design and fabrication

---

# Detector design - overview



Detectors are fabricated using standard microfabrication techniques.

They consist of three main components:

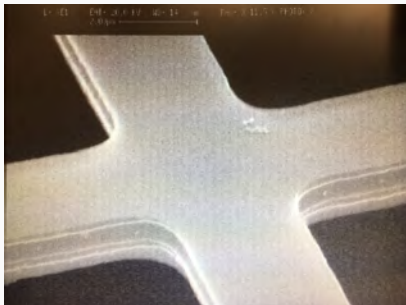
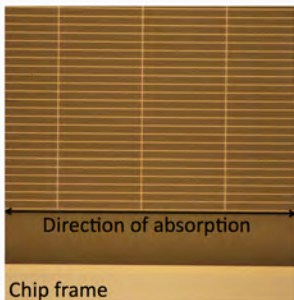
- Absorber structure - absorb single linear polarization
- Endbanks - measure incident optical power with silicon thermistors
- Frame - thermal sink and interface to readout

Each beam's focal plane will consist of two indium bump-hybridized detectors mounted  $< 20 \mu\text{m}$  apart with their absorbers orthogonal.

→ measure orthogonal polarizations of nearly the same electric field.

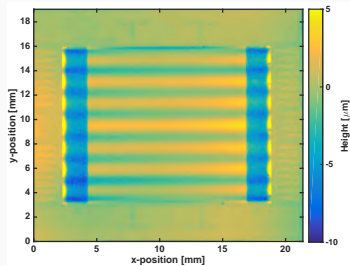
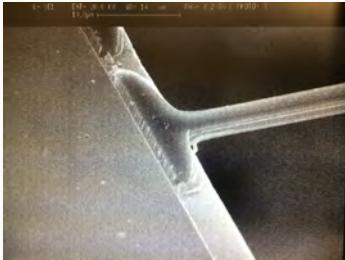


# Absorber structure - overview



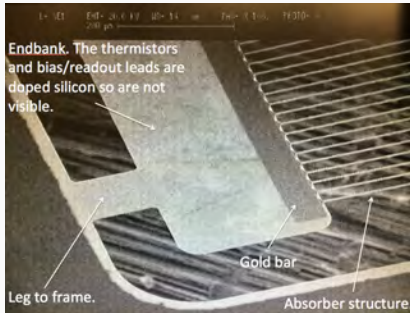
- Consists of a grid of suspended, micromachined, ion implanted silicon wires.
- Wires are degenerately doped to be metallic at all temperatures.
- Effective sheet resistance of the whole structure is  $377 \Omega/\square$ .
- Absorber area sets low frequency cutoff of instrument (15 GHz); grid spacing ( $30 \mu\text{m}$ ) sets high frequency cutoff (5 THz).
- Wire widths and thicknesses are highly uniform across the array.
  - Thickness set by starting SOI device layer thickness ( $1.35 \mu\text{m}$ ).
  - Wires are etched to width with an ICP RIE process.

# Absorber structure - mechanical characterization



- Doping induces compressive stress in absorber wires; previous devices had their wires buckle and protrude up to  $20 \mu\text{m}$  from the frame.  
→ problematic for a hybridized pair of bolometers.
- Detectors subject to vibrations and acoustic excitations at launch.  
→ need resonant frequencies of absorber structure to be much greater than excitation frequencies of launch.
- Solution: deposit highly tensile  $\text{Al}_2\text{O}_3$  film on absorbers outside of active optical region.  
→ Fabricated absorbers are flat and expected to oscillate with amplitudes of  $< 0.4 \mu\text{m}$  rms during launch.

# Endbanks - overview



- Consists of a gold bar for thermalization and two doped silicon thermistors on a crystalline silicon membrane.
  - The gold bar also sets the heat capacity of the endbank.
  - Endbank is formed from the device layer of the SOI substrate.
- Endbanks are connected to the chip frame through eight silicon legs.
  - Thermistors are doped to operate below metal-insulator transition. Electron transport mechanism is variable range hopping [8]:

$$R(T) = R_0 \times \exp \sqrt{\frac{T_0}{T}},$$

where  $R_0$  and  $T_0$  are constants largely determined by geometry and doping, respectively.

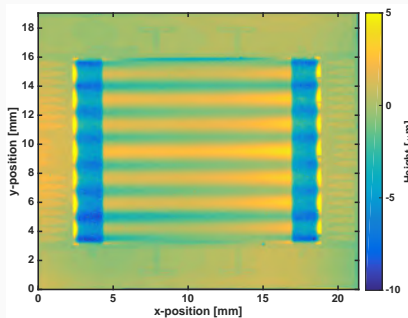


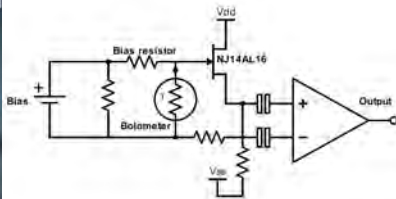
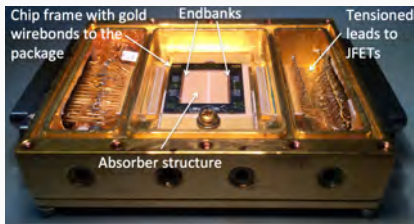
Figure 1: replace this with In bump SEM

- The chip frame is designed so that any two bolometer chips can be hybridized together.
- Large gold-covered areas serve as heat sinks.

## Package and readout

---

# Package and readout - dark tests

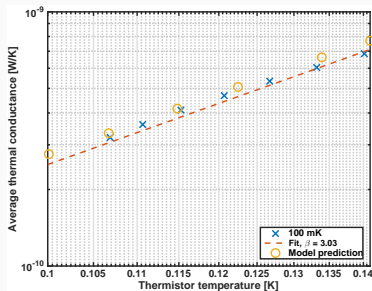
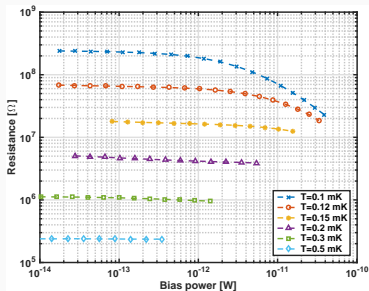


- Thermistor operates under current bias ( $R_{bias} \gg R_{therm}$ ).
- Bolometer is connected to a cryogenic (130 K) JFET amplifier with tensioned leads, mitigating capacitive microphonic contamination of the signal band. We use Interfet NJ14AL16 JFETs that are screened for low noise performance ( $5.5 \text{ nV}/\sqrt{\text{Hz}}$  at 100 Hz).
- Amplifier converts the high source impedance of the thermistors ( $\text{M}\Omega$ -scale) to the low output impedance of the JFETs ( $1.8 \text{ k}\Omega$ ).
- Low impedance signal is AC coupled to a room temperature amplifier.

# Detector performance

---

# Performance - load curves



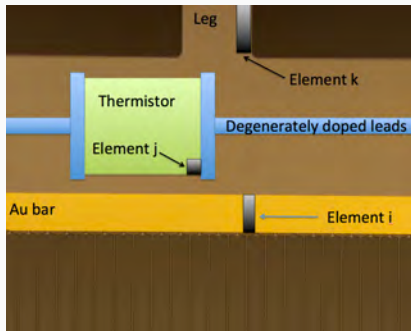
- Determine  $R_0$  and  $T_0$  from the measured resistances under low electrical bias.  
 $\rightarrow T_0 = 15.11 \text{ K}$  and  $R_0 = 911 \text{ } \Omega$ . Operating resistance:  $5.42 \text{ M}\Omega$ .
- Determine average thermal conductance  $\bar{G}$  between the thermistors and the bath from the high-bias end of the load curves:

$$\bar{G} = \frac{P_{\text{bias}}}{T_1 - T_2}. \quad (5)$$

- Fit to the measured  $\bar{G}$  with a function  $\tilde{G} = G_0 \times T^\beta$ .  
 $\rightarrow$  The fit is close to the expected value ( $\beta_{\text{phonon}} = 3$ ).



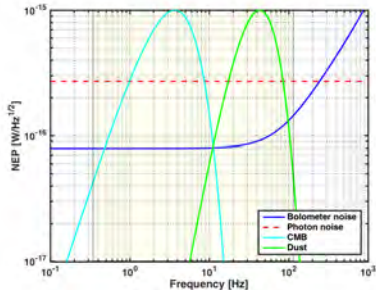
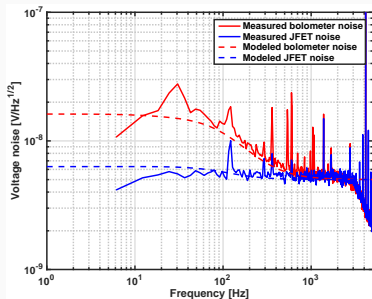
# Performance - thermal model



- For the endbank geometry, break Au bar, thermistors, and legs into small elements.
  - Solve for the etendue  $A\Omega_{ij,ik}$  between all elements.
  - Heat flow between elements (e.g., between i and j) is given by  $P_{ij} = A_{ij} (T_i' - T_j')$ .
- Determine  $G$  between elements, determine  $C$  from material properties/geometries, measure VRH parameters  $R_0$  and  $T_0$ , and solve for non-equilibrium bolometer noise [9]:

$$\text{NEP}_{\text{bolometer}}^2 = \gamma_1 4k_b T^2 G + \frac{1}{S^2} \left( \gamma_2 4k_b TR + e_n^2 + \gamma_3 i_n^2 R + \gamma_4 \text{NEP}_{\text{excess}}^2 \right).$$

# Performance - noise



- Thermal model reproduces the measured  $\bar{G}$  well.
- Modeled noise fits the measured noise well for multiple bias conditions.
- Running the model for the optical and electrical bias conditions expected during flight, we calculate a bolometer NEP of  $7.93 \times 10^{-17} \text{ W}/\sqrt{\text{Hz}}$ .

*Expect to be photon noise limited across the entire PIXIE bandwidth.*

# Conclusions

---

# Conclusions

- We designed, fabricated, and characterized large area polarization-sensitive bolometers for the PIXIE experiment.
- Mechanical characterization of the fabricated PIXIE bolometers shows that the tensioning scheme successfully flattens the absorber strings.
  - Enables indium bump hybridization of a pair of bolometer chips.
  - Mitigates microphonic sensitivity during launch.
- The dark data provide significant insight into the thermal behavior of the endbanks.
  - Thermal model agrees well with the data.
  - The results indicate that the PIXIE bolometers satisfy the sensitivity and bandwidth requirements of the space mission.
- Upcoming work:
  - Characterize the absorber structure (dark measurements of thermal transport and AC impedance, optical measurements with a cryogenic blackbody source.)
  - Subject a hybridized pair of bolometers to environmental testing.



# Acknowledgements

This work was supported by NASA/GSFC IRAD funding. We are especially grateful to the x-ray microcalorimeter group at NASA/GSFC for lending the Astro-E2/Suzaku test platform for PIXIE detector characterization.






# Backup

Backup





# References I

-  A. Kogut, D. J. Fixsen, D. T. Chuss, J. Dotson, E. Dwek, M. Halpern, G. F. Hinshaw, S. M. Meyer, S. H. Moseley, M. D. Seiffert, D. N. Spergel, and E. J. Wollack, “The Primordial Inflation Explorer (PIXIE): a nulling polarimeter for cosmic microwave background observations,” *JCAP* **7**, p. 025, July 2011.
-  A. Kogut, D. T. Chuss, J. Dotson, E. Dwek, D. J. Fixsen, M. Halpern, G. F. Hinshaw, S. Meyer, S. H. Moseley, M. D. Seiffert, D. N. Spergel, and E. J. Wollack, “The Primordial Inflation Explorer (PIXIE),” in *Space Telescopes and Instrumentation 2014: Optical, Infrared, and Millimeter Wave*, *Proc. SPIE* **9143**, p. 91431E, Aug. 2014.
-  D. P. Woody and P. L. Richards, “Near-millimeter spectrum of the microwave background,” *ApJ* **248**, pp. 18–37, Aug. 1981.







## References II

-  H. P. Gush, M. Halpern, and E. H. Wishnow, "Rocket measurement of the cosmic-background-radiation mm-wave spectrum," *Physical Review Letters* **65**, pp. 537–540, July 1990.
-  J. C. Mather, E. S. Cheng, D. A. Cottingham, R. E. Eplee, Jr., D. J. Fixsen, T. Hewagama, R. B. Isaacman, K. A. Jensen, S. S. Meyer, P. D. Noerdlinger, S. M. Read, L. P. Rosen, R. A. Shafer, E. L. Wright, C. L. Bennett, N. W. Boggess, M. G. Hauser, T. Kelsall, S. H. Moseley, Jr., R. F. Silverberg, G. F. Smoot, R. Weiss, and D. T. Wilkinson, "Measurement of the cosmic microwave background spectrum by the COBE FIRAS instrument," *ApJ* **420**, pp. 439–444, Jan. 1994.





## References III

-  G. S. Tucker, H. P. Gush, M. Halpern, I. Shinkoda, and W. Towlson, “Anisotropy in the Microwave Sky: Results from the First Flight of the Balloon-borne Anisotropy Measurement (BAM),” *ApJ* **475**, pp. L73–L76, Feb. 1997.
-  W. A. Holmes, J. J. Bock, B. P. Crill, T. C. Koch, W. C. Jones, A. E. Lange, and C. G. Paine, “Initial test results on bolometers for the Planck high frequency instrument,” *Applied Optics* **47**, pp. 5996–6008, Nov. 2008.
-  B. I. Shklovskii and A. L. Efros, *Electronic properties of doped semiconductors*, vol. 45, Springer Science & Business Media, 2013.
-  J. C. Mather, “Bolometer noise: nonequilibrium theory,” *Applied Optics* **21**, pp. 1125–1129, Mar. 1982.

